Journal of The Electrochemical Society, **155** (1) B70-B78 (2008)
0013-4651/2007/155(1)/B70/9/$23.00 © The Electrochemical Society

Studies of Nafion–$RuO_2 \cdot xH_2O$ Composite Membranes

Catherine Lepiller,[a] Véronique Gauthier,[a] J. Gaudet,[a] A. Pereira,[a] M. Lefevre,[a] Daniel Guay,[a,z] and Adam Hitchcock[b]

[a]*Institut National de la Recherche Scientifique–Énergie, Matériaux et Télécommunications, Varennes, Québec J3X 1S2, Canada*
[b]*Department of Chemistry, McMaster University, Hamilton, Ontario L8S 4M1, Canada*

Nafion/$RuO_2 \cdot xH_2O$ composite membranes were prepared by the recast method. The hydration level of $RuO_2 \cdot xH_2O$ was varied by heat-treatment of commercially available powders, and composite membranes were prepared with various $RuO_2 \cdot xH_2O$/Nafion weight ratios. The through-plane conductivity of the membrane was evaluated in a fuel cell test station (H_2/O_2 at 80°C). The through-plane conductivity decreased from 0.32 to 0.26 Ω cm^2 as a result of the introduction of $RuO_2 \cdot xH_2O$ in the composite membrane. The open-circuit voltage of the single fuel cell element is not affected by the presence of $RuO_2 \cdot xH_2O$ particles. Electrochemical impedance spectroscopy (four-probe method) was also used to evaluate the in-plane conductivity at 80 and 120°C, and at various relative humidities (RHs) ranging from 20 to 90%. In that case, the addition of 5 wt % $RuO_2 \cdot xH_2O$ to Nafion causes a significant increase of the conductivity. The in-plane conductivity does not vary with RH and is unaffected by cation exchange (from H^+ to Ba^{2+} or to Na^+). This is thought to arise as a consequence of $RuO_2 \cdot xH_2O$ sedimentation on one side of the membrane during the casting procedure. This hypothesis was confirmed by point energy-dispersive X-ray analysis and scanning X-ray transmission microscopy that both show the presence of a thin layer (~5 μm) of $RuO_2 \cdot xH_2O$ on one side of the membrane. Scanning transmission X-ray microscopy also reveals that a significant fraction of $RuO_2 \cdot xH_2O$ is incorporated in the bulk of the membrane in the form of isolated aggregates (200–300 nm) made of smaller $RuO_2 \cdot xH_2O$ particles. These aggregates are thought to be responsible for the reduced through-plane ionic conductivity of the composite membrane observed in fuel cell test stations.
 [DOI: 10.1149/1.2803495]

Manuscript submitted June 12, 2007; revised manuscript received September 27, 2007.
Available electronically November 13, 2007.

The current state-of-the-art of polymer electrolyte membrane fuel cell (PEMFC) technology is based on perfluorosulfonic acid (PFSA) membranes operating at an average temperature of 80°C. PFSA ionomers typically consist of a perfluoroalkyl backbone and perfluoroalkyl ether side chains bearing sulfonic acid end groups. Among PFSA membranes, Nafion is recognized for its outstanding properties, including high proton conductivity, excellent chemical stability in both highly oxidative and reductive media (due to its Teflon-like backbone), low gas permeability, and good mechanical strength. Great strides have been made in recent years to decrease both the equivalent weight (EW) and the thickness of Nafion membranes to achieve better durability and higher power density in PEMFCs.

For the past decade, the industrial target has been operation of PEMFCs at higher temperatures to improve the total efficiency and reduce the complexity of the fuel cell ancillary systems. Yet, when used above 80–100°C, Nafion membranes undergo severe structural degradation, including dehydration due to lower affinity for water molecules, loss of dimensional stability due to irreversible softening of the polymer backbone near the glass transition temperature, and higher fuel permeation.

Mixing of Nafion with various fillers has been proposed as a way to improve water retention at low humidification and/or higher temperatures, and to improve proton transport. Three main approaches have been followed and they have recently been reviewed.[1-4] These approaches include: (*i*) impregnating or casting with free nonvolatile acids,[5] heteropolyacids (HPAs),[6-13] or ionic liquids,[14] (*ii*) reducing the thickness of the membranes by the Teflon-based microreinforcement technique,[15-20] and (*iii*) preparing organic/inorganic composite membranes with Nafion and hygroscopic oxides such as SiO_2,[21-30] ZrO_2,[29,30] Al_2O_3,[22,30] and TiO_2,[28,29,31-33] or solid inorganic proton conductors such as zirconium phosphate[26,34-37] and cesium phosphate.[1]

The properties of these membranes can be further improved by combining some of the approaches described above. For example, approaches (*i*) and (*iii*) were used to stabilize water-soluble HPA additives by ion exchange of the protons with larger cations,[11,12] or by supporting it onto high-surface-area silica.[13,26-28] Likewise, approaches (*ii*) and (*iii*) were used together to prepare composite Nafion–Teflon–$Zr(HPO_4)_2$ membranes derived from 25 μm thick Gore-Select membranes, which are routinely obtained by impregnating a Nafion solution into a microporous Teflon matrix.[15] Besides better mechanical strength, the resulting membrane has a higher conductivity, which was ascribed to both a reduction of the membrane thickness and the presence of extra proton-exchange sites due to the incorporation of zirconium phosphate.[16]

Another interesting approach to improve the performance of membranes under low-humidity conditions is the concept of self-humidification.[38] It basically consists of dispersing Pt nanoparticles that catalyze the recombination of crossover hydrogen with oxygen to generate water molecules in situ in the bulk of the membrane. This results in more stable fuel cell operation at 80°C without any external humidification.[39] This approach was further developed by combining the effects of Pt and hygroscopic SiO_2,[39,40] TiO_2,[33] or using Pt/SiO_2 nanoparticles.[18,19,39]

In the course of these various studies, composite membranes were prepared by either recasting from a Nafion ionomer solution mixed with the desired solid or a sol-gel approach based on the in situ chemical precipitation of solid nanoparticles inside the hydrophilic pores of a commercial membrane. It is not clear which approach should be preferred; except for one study,[4] most papers on the subject have reported comparable results.[23,24,29,33,35] Nevertheless, the particle size of the solid additives proves to be important to maximize the surface-to-volume ratio and to increase the interaction with the ionomer to bridge the hydrophilic clusters more effectively.[1,9,11,29,30,37]

There is general agreement in the literature that the incorporation of hydrophilic additives enhances water uptake and imparts better thermal stability to the composite membrane.[2] However, despite higher water retention properties, the proton conductivity of the hybrid membranes are often lower than, or at most equal to, that of bare Nafion membranes.[8,11,25,26,35-37] In the case of zirconium phosphate, this observation was explained by a "scaffolding effect" of the additive that would account for a greater rigidity of the membrane by constricting the pores through polymer-additive interactions.[36] In any case, increased proton conductivity is generally observed for nanosized particles as opposed to larger particles.[9,29,31,33,39] Proton transport in composite membranes occurs

[z] E-mail: guay@emt.inrs.ca

through a complex interplay between the surface and chemical properties of the polymer and the additives,[1,26] and the use of "bifunctional" additives, which are both hygroscopic and able to conduct protons, should require special attention.

In this paper, we choose to concentrate on hydrous ruthenium oxide, $RuO_2 \cdot xH_2O$, a mixed electronic–protonic conductor, as an additive to Nafion. Ruthenium oxide belongs to a class of oxides that encompasses many transition-metals or rare-earth oxides. Proton conduction in these oxides occurs by a mixed-translocation mechanism, whereby protons move along an adsorbed hydrous structure.[41] This material is considered to be one of the best electrode materials for electrochemical capacitors due to its high specific pseudocapacitance, high conductivity, and reversibility. More importantly, the proton dynamics of $RuO_2 \cdot xH_2O$, which have been characterized by variable-temperature ^1H spin-lattice relaxation time (T_1) measurements,[42] are excellent. Upon varying the hydration state x of the hydrous ruthenium oxide powder through heat-treatment, a minimum of the proton activation energy was found for powders annealed between 100 and 200°C. This minimum was correlated with a maximum of specific capacitance.[42] Other studies have confirmed that the charge-storage and electrocatalytic properties of $RuO_2 \cdot xH_2O$ strongly depend on structural water content.[43-46] According to Dmowski's nanocomposite structural model,[43] metallic conduction is supported by the oxide rutile-like nanocrystals, while proton conduction is associated with water chemisorbed along grain boundaries with oxides.

Given the importance of the hydration state of $RuO_2 \cdot xH_2O$ for the conduction of protons, we accordingly have assessed the properties of different Nafion/$RuO_2 \cdot xH_2O$ composite membranes prepared by the recasting method. The water content x was varied by heating commercially available powders at different temperatures. These composite membranes were tested in a H_2/O_2 polymer electrolyte membrane fuel cell test station. Conductivity profiles at 80 and 120°C were established in a four-electrode conductivity cell, and the structural organization and dispersion of the oxide particles in the composite membranes were assessed through a combination of scanning electron microscopy and scanning transmission X-ray absorption microscopy.

Experimental

Membrane preparation.— Membranes (wet thickness between 65 and 95 μm) were prepared by solution casting. The casting solvent was composed of a 3:1:1 mixture of 2-propanol/water/*N*,*N*-dimethylformamide (DMF), unless otherwise stated. Dimethylformamide and 2-propanol (ACS certified) were purchased from Fisher Chemicals and Sigma-Aldrich, respectively. The addition of DMF, a high-boiling solvent, has been reported to improve the mechanical strength and plasticity of the recast membranes.[8,47-50] Other high-boiling point solvents, like dimethylsulfoxide (DMSO) and ethylene glycol, have a similar effect. In the present series of experiments, DMF was selected because it allows the application of a moderate heating step above the Nafion vitreous transition temperature ($T_g \sim 110$°C[51]) at the end of the casting process. This heating step was proposed to replace the classical heating post-treatment above T_g that is necessary to induce a structural reorganization of the polymer chains and to achieve good mechanical properties.[52]

Hydrated ruthenium(IV) oxide (Ru content 54% min), $RuO_2 \cdot xH_2O$, was purchased from Alfa Aesar. The commercial powder was partially hydrated and is best described as $RuO_2 \cdot xH_2O$, with $2 < x < 3$. It was heated in air for 24 h at three different temperatures, i.e., 75, 150, and 400°C, to remove some of the structural water molecules and to study the influence of the hydration level on the conductivity of the composite membranes. It is generally assumed that complete dehydration of $RuO_2 \cdot xH_2O$ occurs above 350°C.[53] Considering that a thermal treatment at 400°C gives anhydrous RuO_2, it is possible to determine the water content of $RuO_2 \cdot xH_2O$ heated at 75 and 150°C by determining the weight loss of the sample upon subsequent heating at 400°C. Using this procedure, it was found that $x = 2.12$ for as-received $RuO_2 \cdot xH_2O$, and that $x = 1.94$ and 0.51 for $RuO_2 \cdot xH_2O$ annealed at 75 and 150°C, respectively. The extent of partial dehydration observed at 150°C is in good agreement with literature data. For instance, Ref. 43 found $x = 0.58$ for $RuO_2 \cdot xH_2O$ treated under the same annealing conditions, while $x = 0.50$ and 0.44 were found in Ref. 54 and 55 for $RuO_2 \cdot xH_2O$ annealed at 150°C for 17 h. The hydration level for as-received $RuO_2 \cdot xH_2O$ powder is also consistent with former determinations (for instance, $x = 2.11$ in Ref. 43 and $x = 2$ in Ref. 54). Prior to their use, the three powders were ground using an agate mortar and pestle.

The structure of the heat-treated $RuO_2 \cdot xH_2O$ powders was studied by X-ray diffraction (XRD) (the diffractograms are not displayed). The X-ray diffractogram of fully hydrated $RuO_2 \cdot xH_2O$ displays very broad diffraction peaks that are characteristic of either an amorphous or a nanocrystalline structure. Similar X-ray diffractograms were obtained for $RuO_2 \cdot xH_2O$ heat-treated at 75 and 150°C. In contrast, much sharper diffraction peaks, corresponding to the rutile structure of RuO_2, are observed for the powder annealed at 400°C, consistent with what was found elsewhere.[56] The presence of these sharper peaks indicates that the loss of hydration water molecules causes a partial ordering of the RuO_2 unit. These results are consistent with data from the literature showing that diffraction peaks are almost absent in the XRD patterns of $RuO_2 \cdot xH_2O$ powders heated at temperature below 200°C.[43,46,57] Upon increasing the temperature, removal of structural water molecules causes a structural reorganization of the compound and a partially ordered three-dimensional rutile network is formed.

The preparation procedure of the composite membranes was as follows: 2 g of 20 wt % Nafion dispersion (EW 1050 equiv g^{-1}) from DuPont were weighed and mixed with the ternary solvent composed of 9 mL 2-propanol + 3 mL Millipore water + 3 mL DMF. For RuO_2-based composite membranes, the proper amount of $RuO_2 \cdot xH_2O$ powder was added to the ionomer solution. Two series of membranes with different $RuO_2 \cdot xH_2O$ loadings were prepared. The first series contained 1 wt % $RuO_2 \cdot xH_2O$ (based on the weight of RuO_2), while the second series contained 5 wt % $RuO_2 \cdot xH_2O$. To account for the different hydration state of the powders, the added mass of $RuO_2 \cdot xH_2O$ was based on that of the dehydrated RuO_2 content. The mixture of $RuO_2 \cdot xH_2O$ powder and Nafion was briefly stirred with a magnetic bar and then sonicated for 30 min. High-shear mixing of the dispersion for 3 h was explored for some early preparations. No substantial improvement of the membrane's compositional homogeneity was achieved by high-shear mixing compared to ultrasonication, and that later method was eventually preferred. The slurry was then poured into a circular casting mold. This homemade mold consists of a cylindrical hollow glass piece (i.d. 5.4 cm, i.e., surface area 22.9 cm^2) that is deposited onto a flat glass support of larger surface area. The whole set is clamped tightly between two square stainless steel pieces with two intercalated Teflon O-rings (Chemglass).

The solvent was evaporated by heating the samples according to the following sequence. First, the sample was brought to 80°C over 90–100 min. It was then brought slowly (over a period of 50–60 min) to 140°C and held at 140°C for 10 min. This last step imparts insolubility to the recast films.[58] As-prepared membranes were allowed to cool to room temperature overnight, and they were peeled from their glass support under deionized water the next day. Parts of the membranes were analyzed in the Na^+ form; therefore, they were only boiled for 1 h in deionized water before conductivity measurements. The protonation treatment consisted of washing the membranes for 1 h in hot 3% hydrogen peroxide solution, rinsing for 1 h in boiling deionized water, proton-exchanging for 1 h in boiling 1 M sulfuric acid, and finally, rinsing for one additional hour in boiling deionized water.[59] For membranes in the Ba^{2+} form, an additional H^+/Ba^{2+} ion-exchanged step in hot 0.1 M $BaCl_2$ ($BaCl_2 \cdot 2H_2O$ from Anachemia) for 1 h, followed by rinsing for 1 h

in boiling deionized water, was carried out after the protonation step described above. All membranes were stored at ambient temperature in deionized water until further use.

Membrane and powder characterization.— The chemical profile of the composite membranes was determined using the energy-dispersive X-ray (EDX) spectrometer attachment of a scanning electron microscope (JEOL JSM-6300F). Membranes in swollen state were freeze-fractured in liquid N_2, exposing a fresh cross-sectional surface. Pieces were fixed onto a silicon substrate with a copper tape and attached to the sample support with a carbon-based paste. The F, S, and Ru composition profiles were determined by probing F/S and Ru/S atomic ratios measured at an accelerating voltage of 20 kV and a magnification of $\times 5000$ at several points evenly distributed across the membrane thickness.

The interferometrically controlled scanning transmission X-ray microscope (STXM)[60] at bending magnet beamline 5.3.2 at the Advanced Light Source (ALS)[61] was used for chemical mapping using X-ray absorption. The methods of measuring and analyzing STXM images and spectra have been described elsewhere.[62,63] The aXis2000 program[64] was used to process the spectral and image data. For STXM, the samples were cut to 2–3 μm thick slices and deposited on a thin Si_3N_4 window.

Fuel cell testing.— Nafion/5% $RuO_2 \cdot 1.94H_2O$ and Nafion/5% RuO_2 composite membranes were prepared and equilibrated as described above. They were used as electrolyte in a H_2/O_2 PEMFC operated at 80°C/100% relative humidity (RH). The performance was compared to plain, commercially available and recast Nafion membranes under the same experimental conditions.

Commercial ELAT disks from E-TEK (surface area 1.13 cm^2) supporting a platinum catalyst layer of 0.4 mg cm^{-2}, i.e., 20 wt %, served both as electrodes and gas diffusion layers (GDLs). Nafion dispersion was paint-brushed onto the surface of the anode and the cathode to improve interfacial three-phase contact between the membrane and the electrodes. The mass deposited was of the order of 0.5–1 mg cm^{-2}. The catalyzed GDLs were dried on a hot plate at 100°C for a few minutes before subsequent membrane electrode assembly (MEA) buildup.

The MEAs were fabricated by sandwiching the different membranes between two identical ELAT electrodes and hot-pressing at 140°C and 300 psi for 40 s. They were placed between two Teflon gaskets in fuel cell hardware from Globetech, Inc. The single fuel cell was run at 80°C and fed on the anode side with hydrogen (pressure 30 psig, flow rate 500 cm^3 min^{-1}) and on the cathode side with oxygen (pressure 60 psig, flow rate 500 cm^3 min^{-1}). The system was pressurized and both gases were fully hydrated before entering the fuel cell by passing through humidification bottles set at 110°C. All running parameters were fixed, controlled, and registered by a Hewlett-Packard 6060B test station.

The MEAs were equilibrated at a constant potential of 0.5 V vs a reversible hydrogen electrode (RHE) for 20 h. This step was necessary to electrochemically clean the Pt catalyst surface, reach optimal hydration of the membrane using the water produced by the electrochemical reaction, and obtain stable polarization curves.

Conductivity measurements.— The experimental setup developed for the measurement of the specific conductivity is adapted from the four-electrode ac impedance method developed by Sone et al.[59] However, several improvements were made compared to the original system, and our system allows for a precise control of the humidity over the whole 0–100% humidity range and for temperatures up to 150°C. The home-built conductivity measurement system is composed of four conductivity cells able to run simultaneously under nitrogen atmosphere. One of the cells is back-pressurized to control the humidity levels at temperatures higher than 100°C. A short description of the conductivity measurement system follows.

The conductivity was measured by electrochemical impedance spectroscopy (EIS) using a four-electrode configuration cell. The conductivity cell is made of four parallel Pt wires (Alfa Aesar, diameter 0.25 mm), equally spaced on a plastic support. The two outer Pt wires (3 cm apart) are used to impose an ac potential, while the two inner Pt wires (1 cm apart) are used to measure the ac current. The plastic support encasing the four parallel Pt electrodes is made of temperature-resistant Kel-F polymer. A "window"-type cell design, with large voids (holes) between the electrodes, makes possible the rapid humidification of the membrane by direct contact with the circulating humidified gas. Membrane strips (3.0–3.5 cm $\times$ 0.8–1.1 cm) were cut from the wet membranes and placed symmetrically on top of the Pt electrodes. To complete the cell, a second plastic support was clamped on top of the bottom support and held in place with screws.

The conductivity cell was introduced in a stainless steel chamber that was itself fixed inside an Isotemp oven (Fisher, model RH202P) by quick connects (Swagelok). Electrical contact was established by heat-resistant connectors and cables. The temperature was controlled within ±0.3°C. The atmosphere in the stainless steel chamber was controlled by circulating a humidified nitrogen gas (N_2 flow was adjusted at 300 cm^3 min^{-1} with mass flowmeters). The N_2 gas was humidified by circulating it through a heated glass reaction pressure flask (Lasalle Scientifique, Inc.) containing water. The vapor pressure in the circulating N_2 gas is controlled by adjusting the temperature of water in the glass reaction pressure flask. The humidified gas was then circulated through the stainless steel chamber and the open configuration of the conductivity cell enabled direct exposure of the membranes to the humidified gas. Rope heaters (Omega) maintained at 10°C above the working MEA prevented water condensation in the stainless steel tube connecting the glass reaction pressure flask and the stainless steel chamber. Control of the temperature profiles and data acquisition was performed via a resistance thermometer device (RTD) temperature probe controlled by a software-managed controller system (model ZCP403 manufactured by Zesta Engineering, Ltd.). Water heating in the glass reaction pressure flask was achieved through a temperature ramp of 1°C min^{-1} up to final temperature. The set value was then maintained with an accuracy of ±0.1°C. The equilibration time of commercially available recast Nafion and Nafion–RuO_2 composite membranes was about 4–5 h after starting the heating process.

The impedance of the membranes (in-plane conductivity) was measured at open-circuit potential using a Solartron SI 1255 HF frequency response analyzer, combined with a Solartron multipotentiostat (model Multistat 1480A), over a frequency range extending from 10^{-1} to 10^5 Hz (5 mV ac amplitude). The specific conductivity of the membranes, σ (S cm^{-1}), was determined by taking the average of the real part, R, of the complex impedance over a frequency range extending from 10^1 to 10^4 Hz (the phase angle is zero over that range). Conductivity values were obtained from Eq. 1

$$\sigma = l/RS \qquad [1]$$

where l (cm) denotes the distance between the reference electrodes (1 cm) and S (cm^2) is the cross-sectional area of the membrane. The thickness of the membranes was determined with a numeric micrometer (Geneq, Inc., model 1060001). The accuracy of each measurement is ±4 μm. For each RH/T condition, several series of 20 consecutive impedance spectra were taken on equilibrated membranes and the final conductivity was calculated from the average resistance value.

Results

Fuel cell testing.— The performances of the various membranes were verified in a bench scale fuel cell test station. Figure 1 shows the cell potential (E) vs current density (j) curves for different H_2/O_2 single fuel cells fabricated from commercially available and recast Nafion membranes, and Nafion/5% RuO_2 and Nafion/5% $RuO_2 \cdot 1.94H_2O$ composite membranes. All measurements were performed at 80°C under fully humidified conditions (see Experimental section). As seen in Fig. 1, the current densities for composite mem-

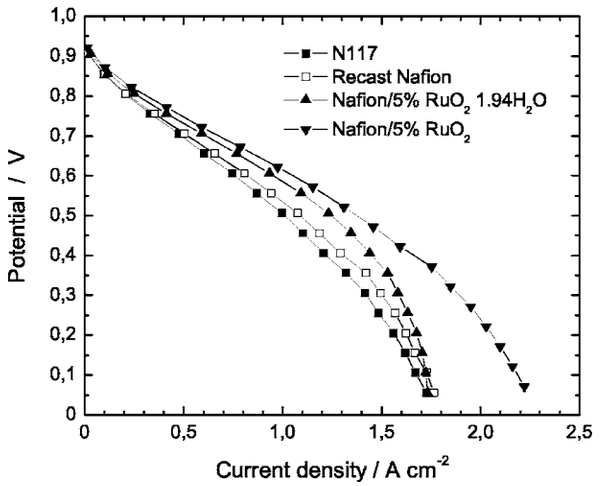

Figure 1. Polarization curves of Nafion/5% RuO_2 and Nafion/5% $RuO_2 \cdot 1.94H_2O$ composite membranes measured at 80°C. Also shown are the polarization curves of commercially available and recast Nafion membranes.

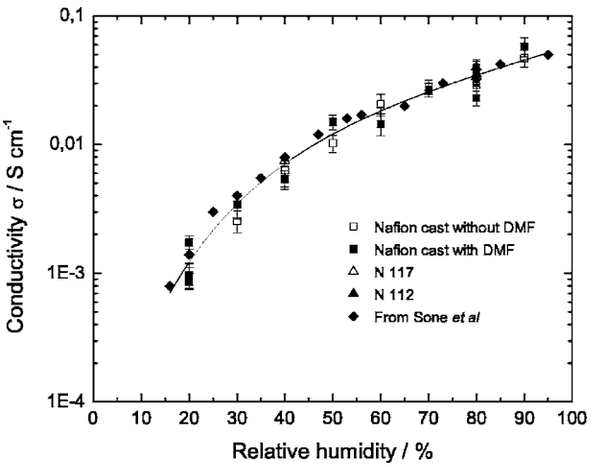

Figure 2. Conductivity profiles of Nafion membranes measured at 80°C.

branes exceed that of the bare Nafion membranes at all cell potentials. The performance of a single fuel cell is thus improved by the introduction of $RuO_2 \cdot xH_2O$ in the membrane. This is especially the case for the MEA prepared with a Nafion/5% RuO_2 composite membrane. More severe mass-transport limitations at the highest current densities are observed for the Nafion/5%·1.94RuO_2 composite membrane, but this might be due to a nonoptimized procedure of preparing the MEA.

All polarization curves were analyzed by fitting the experimental data to Eq. 2

$$E = E_0 - b \log j - Rj \quad [2]$$

where E is the observed cell potential, E_0 is the open-circuit potential, b is the Tafel slope, j is the current density, and R is the total resistance of the cell. Equation 2 above does not take into account mass-transport limitations occurring at the highest current densities and so the polarization curves were fitted up to 1 A cm^{-2}, where mass-transport limitations are not severe. The parameters extracted from the fitting of the curves are given in Table I.

As seen in Table I, open-circuit potential (OCP) values are very close to each other, with a mean value of 0.958 V. Interestingly, the fact that the OCP values are the same for cells prepared using either Nafion or Nafion/5% $RuO_2 \cdot xH_2O$ composite membranes indicates that the gas permeability of the membrane is not affected by the introduction of $RuO_2 \cdot xH_2O$ and that short-circuiting of the anode and cathode is not an issue. Also, there is a small difference between the Tafel slopes of the MEAs made from Nafion/5% $RuO_2 \cdot xH_2O$ composite membranes (~40 mV/dec) as opposed to those made from bare Nafion membranes (~30 mV/dec). However, this small difference might not be significant and may arise simply as a consequence of the limited current range (<1 A cm^{-2}) used to fit the polarization curves.

Table I. Values of the electrokinetic parameters obtained from the polarization curves measured at 80°C.

Membrane	E_0 (V)	b (mV/dec)	R (Ω cm^2)
N117	0.958	31	0.35
Recast Nafion	0.958	28	0.32
Nafion/5% $RuO_2 \cdot 1.94H_2O$	0.950	40	0.26
Nafion/5% RuO_2	0.966	39	0.25

It is also noteworthy that the total resistance, R, is about 25% lower for MEAs made with RuO_2-based composite membranes compared to reference MEAs using bare Nafion. Considering that the various cells were made in a similar manner and that only the nature of the membrane is changed, this implies that there is a significant decrease of the resistance associated with the transport of protons in the composite membranes. The R values of the composite membranes are 0.25–0.26 Ω cm^2, which is comparable to the value of 0.26 Ω cm^2 obtained by Adjemian et al. with a recast Nafion/10% SiO_2-based MEA under the same experimental conditions.[24] In the following section, we investigate in more detail the conductivity behavior of the composite membranes with respect to RH.

Conductivity measurements.— The conductivity measurement system was calibrated at 80°C with recast Nafion membranes, and the experimental values were compared with commercially available Nafion membranes (N117 and N112) and with literature data. As stated previously, recast Nafion membranes were prepared with the addition of DMF in the casting solution and included a post-treatment at 140°C. The conductivity profile (80°C) of the recast-Nafion membrane is plotted in Fig. 2 as a function of RH. For the sake of comparison, the conductivity profile of a recast-Nafion membrane prepared without the addition of DMF is also shown. Also depicted in that figure are the conductivity profiles of commercially available Nafion membranes and the data taken from Sone et al. for Nafion N117 at 80°C.[59]

As seen in Fig. 2, the conductivity profiles of both recast Nafion membranes (with and without the addition of DMF) are very close to each other, indicating that the addition of DMF has no peculiar deleterious or beneficial effect on the protonic transport of recast Nafion membrane. These values are also similar to those measured on commercially available N117 or N112 Nafion membranes. The cluster-network microstructure of recast Nafion membranes is most unaffected by the presence of DMF in the casting solution and is most probably similar to that of the extruded form of the membrane. Incidentally, the conductivity values measured on commercially available Nafion membranes are similar to those obtained by Sone et al.,[59] confirming the validity of our experimental approach. To set a reference point, the mean ionic conductivity at 80°C/80% RH is 0.035 S cm^{-1}, and the standard deviation, based on 50 different measurements made on 20 different membranes, is 0.005 S cm^{-1}.

The conductivity vs RH profiles of Nafion/5% $RuO_2 \cdot xH_2O$ composite membranes are shown in Fig. 3 for various values of x. The conductivity profiles of Nafion/5% RuO_2 and Nafion/5% $RuO_2 \cdot 0.51H_2O$ composite membranes are surprisingly flat over the whole RH range, with mean σ values of 0.328 and 0.166 S cm^{-1}, respectively. These values are much larger than the conductivity

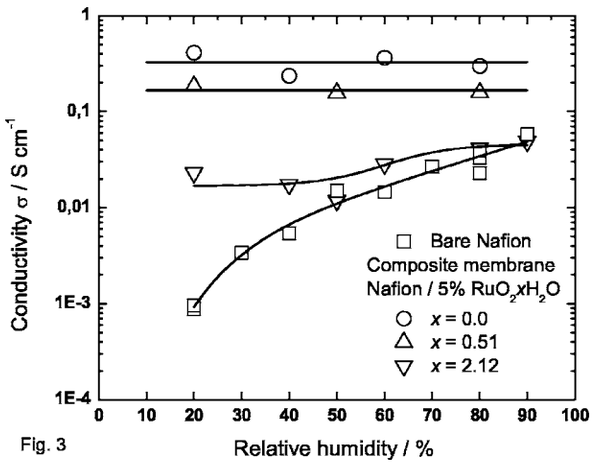

Figure 3. Influence of the hydration state of ruthenium oxide on the conductivity profile of Nafion/5% $RuO_2 \cdot xH_2O$ composite membranes. The conductivity profile of bare Nafion membrane is also shown. All measurements were realized at 80°C.

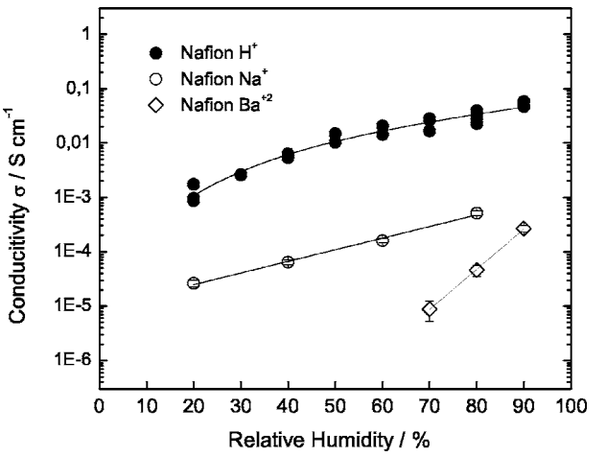

Figure 4. Influence of the ionic form of recast Nafion membranes on their conductivity profile at 80°C.

measured on bare Nafion membranes. For these two membranes, the water vapor pressure has very little effect on the in-plane conductivity. The hopping of protons through water molecules is definitely less important for these composite membranes than it is for bare Nafion membranes. An alternative conduction pathway through the oxide particles needs to be invoked to explain the invariance of the conductivity on the RH values. In the case of the Nafion/5% $RuO_2 \cdot 2.12H_2O$ composite membranes, the conductivity profile is close to that of bare Nafion for RHs $\geqslant$ 50%. For smaller RH values ($<$50%), the conductivity values are almost constant ($\sim$0.02 S cm^{-1}), much larger than that of bare Nafion membranes.

In order to examine the influence of temperature, additional measurements were performed at 120°C on Nafion/5% $RuO_2 \cdot 0.51H_2O$ composite membranes at low RH (20%) and high RH (80%). As seen in Table II, there is no difference between the conductivity measured at 20% RH and 80% RH. For comparison, the conductivity of bare Nafion membranes measured under the same conditions varies from 0.0026 and 0.0615 S cm^{-1} as RH increases from 20 to 80%.

Nafion/1% $RuO_2 \cdot xH_2O$ (instead of 5 wt %) composite membranes were also cast using RuO_2, $RuO_2 \cdot 0.51H_2O$, and $RuO_2 \cdot 2.12H_2O$. The conductivity value of any of the Nafion/1% $RuO_2 \cdot xH_2O$ composite membranes does not differ by more than 10% from that of bare Nafion membranes. Conductivity vs RH profiles of these membranes are identical to each other and closely follow that measured on bare Nafion membranes. This difference is well within the experimental uncertainty (see above), and it must be concluded that the addition of 1 wt % of $RuO_2 \cdot xH_2O$ to the Nafion solution does not affect the conductivity of the resulting membrane.

It was hypothesized that the electronic conductivity of the oxide additive might contribute significantly to the overall conduction seen in Nafion/5% $RuO_2 \cdot xH_2O$ composite membranes. To separate the ionic and electronic contributions from the measured signal, we have changed the nature of the counterion associated with the sulfonic acid groups of the ionomeric membrane. For this purpose, protons were ion-exchanged with Na^+ and Ba^{2+} ions as described in the Experimental section and the conductivity of the membrane in the Na^+ and Ba^{2+} forms was measured as a function of RH.

Figure 4 shows the conductivity vs RH profile of bare Nafion membranes in three different forms, namely, H^+, Na^+, and Ba^{2+}. As seen in Fig. 4, the σ values are greatly affected by the nature of the cation. The conductivity of the Na^+-exchanged Nafion membrane is about 2 dec lower than the conductivity of the bare Nafion membrane in the H^+ form. The conductivity is even lower for the bare Nafion membrane in Ba^{2+} form, and the slope of the conductivity vs RH curve is steeper than for the other two forms. Nafion membranes in Ba^{2+} form become highly resistive as the RH values decrease, and it was not possible to measure σ values for RH values lower than $\sim$70%. It is assumed that proton transport in both Na^+- and Ba^{2+}-ion-exchanged Nafion membranes is hindered by electrostatic effects arising from the double positive charge of Ba^{2+} and steric effects due to the larger size of the cation.

The conductivity results of Nafion/5% $RuO_2 \cdot xH_2O$ composite membranes in H^+, Na^+, and Ba^{2+} forms are displayed in Fig. 5a (x = 0), 5b (x = 0.51), and 5c (x = 2.12), respectively. In all cases, the conductivity vs RH profiles are flat and do not vary with RH. There is little variation of the conductivity when the counterion is changed from H^+ to Na^+ and then to Ba^{2+}. In the case of Nafion/5% RuO_2 composite membranes (Fig. 5a), the conductivity increases slightly from H^+ to Na^+ and then to Ba^{2+} form. For Nafion/5% $RuO_2 \cdot 0.51H_2O$ membranes (Fig. 5b), all conductivity curves are superimposable, whereas for Nafion/5% $RuO_2 \cdot 2.12H_2O$ membranes (Fig. 5c), no clear trend is observed. The invariance of the conductivity value with RH is also verified at 120°C (see Table II). The contrast observed between the results of Fig. 4 (pronounced dependency of σ on RH as the cation is changed) and Fig. 5 (no change in the σ value with RH as the cation is changed) is a strong indication that proton conduction is probably not the main conduction mechanism involved in the in-plane conductivity of Nafion/5% $RuO_2 \cdot xH_2O$ membranes.

Table II. Conductivities for Nafion/5% $RuO_2 \cdot 0.51H_2O$ composite membranes at 120°C.

Relative humidity (RH)	σ in H^+ form (S cm^{-1})	σ in Na^+ form (S cm^{-1})
20%	0.163 ± 0.014	0.168 ± 0.017
	0.168 ± 0.017	0.141 ± 0.018
80%	0.163 ± 0.018	0.155 ± 0.017

Membrane characterization.— Figure 6 shows the cross-sectional Ru/S and F/S atomic ratios of a Nafion/5% $RuO_2 \cdot 0.51H_2O$ composite membrane, determined by X-ray fluorescence analysis in a scanning electron microscope (SEM-EDX). In that case, dispersion of the ruthenium oxide powder was achieved by high-shear mechanical mixing of the slurry at constant speed for 3 h, followed by ultrasonication for half an hour just prior to pouring the solution into the glass mold. As expected, the membrane exhibited uniform F/S atomic ratio (63.4 ± 4.8%) across the whole

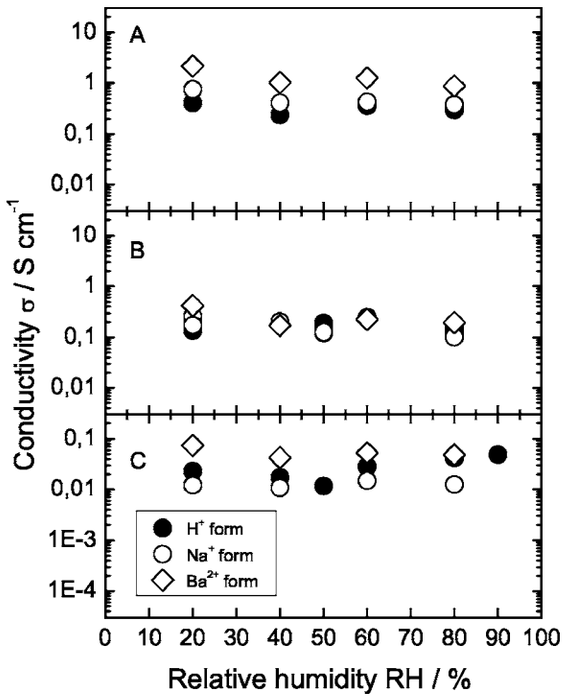

Figure 5. Influence of the ionic form of Nafion/5% $RuO_2 \cdot xH_2O$ composite membranes on the conductivity profile: (A) $x = 0$, (B) $x = 0.51$, and (C) $x = 2.12$. All measurements were realized at 80°C.

section of the membrane. In the case of Ru and S, the Ru/S atomic ratio is constant across the membrane (0.30 ± 0.06%), except for a nearly fivefold enrichment of ruthenium (Ru/S = 1.49%) on one side of the membrane. Looking back at the way the membrane was cast, it was realized that the side of the membrane that exhibits Ru enrichment is the one that was in contact with the glass plate during the casting process. The same analysis performed on a membrane prepared without any high-shear mixing gave similar results (not shown here). The presence of a Ru-enriched layer at the bottom face of the membrane indicates that partial sedimentation of $RuO_2 \cdot xH_2O$ occurs during casting of the membrane. Casting of the membrane is a very slow process that occurs over a period of two days. Through a series of SEM micrographs (not shown), it was possible to estimate the thickness of the Ru-enriched layer. The Ru-enriched layer is between 5 and 10 μm thick and does not vary much from one composite membrane to the other.

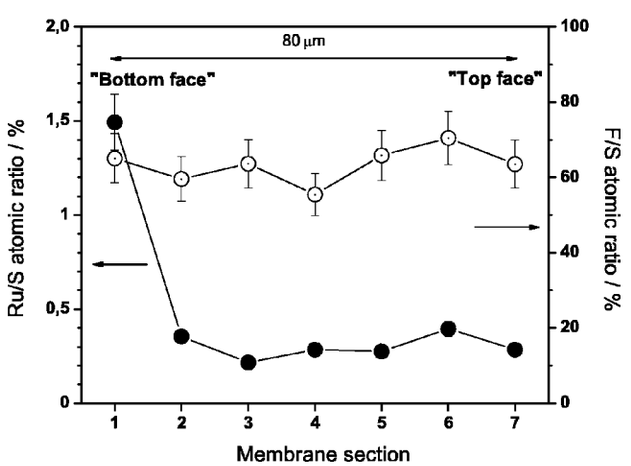

Figure 6. Cross-sectional composition profile of a recast Nafion/5% $RuO_2 \cdot 0.51H_2O$ membrane determined by X-ray fluorescence analysis in a scanning electron microscope (SEM-EDX). The membrane is 80 μm thick.

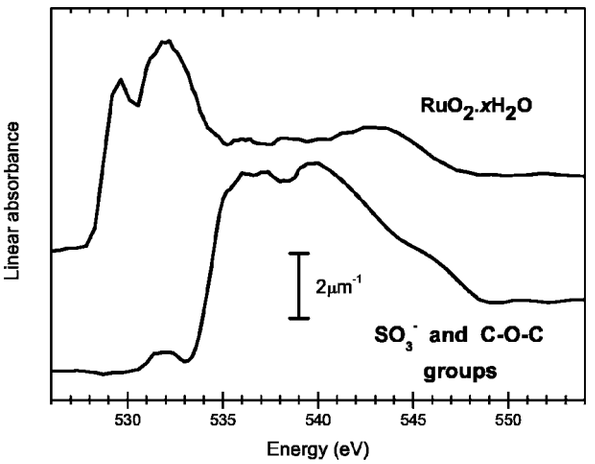

Figure 7. O K-edge spectra of $RuO_2 \cdot xH_2O$ and of PFSA polymer extracted from image sequences recorded using STXM on a recast Nafion/5% $RuO_2 \cdot 0.51H_2O$ membrane.

It was not possible to detect $RuO_2 \cdot xH_2O$ aggregates in the bulk of the membrane by relying on SEM and EDX. However, STXM was able to directly visualize both the Ru-enriched sedimentation layer and also $RuO_2 \cdot xH_2O$ aggregates in the bulk of the membrane. As described elsewhere,[62,63] STXM provides both spectroscopic and spatial information and thus allows unambiguous identification of $RuO_2 \cdot xH_2O$ aggregates within the bulk of the membrane, with clear differentiation of them from the surrounding polymer.

Figure 7 presents the O K-edge spectra of bare $RuO_2 \cdot xH_2O$ and pure Nafion, which are quite different. In the case of $RuO_2 \cdot xH_2O$, the O K-edge displays two sharp absorption features at 529.8 and 531.5 eV. While detailed interpretation of these spectral features requires calculations, generally speaking, they can be ascribed to excitations from the O 1s level to the empty p-density of states of RuO_2. The associated water signal is not identifiable. The O K-edge spectrum of liquid water[65] is dominated by a broad band peaking at 538 eV with a pre-edge peak at ~535 eV. In contrast, the SO_3^- moiety and the two ether groups (–C–O–C–) of the PFSA ionomer display only a small absorption feature at 531.5 eV below the O absorption K-edge dominated by a broad peak attributable to O 1s $\rightarrow \sigma^*_{S=O}$ excitations centered at 538 eV. It is thus possible to use the O K-absorption spectra in a fingerprint fashion to identify these compounds, to map their spatial distributions in fuel cell membranes, and to unequivocally discriminate between regions of the membrane that are either $RuO_2 \cdot xH_2O$- or Nafion-rich.

Figure 8a shows an image obtained at 520 eV in a region close to the surface of the composite membrane. As seen in that image, the composition at the surface of the composite membrane is different from that of a few micrometers away. On that scale, the composition of the bulk of the composite membrane is homogenous. However, detailed analysis reveals the presence of $RuO_2 \cdot xH_2O$ aggregates dispersed in the Nafion matrix (see later).

In order to provide a detailed chemical analysis, images of a region of a Nafion/5% $RuO_2 \cdot xH_2O$ composite membrane were recorded at a series of energies across the O K-absorption edge from 526 to 560 eV (image sequence or "stack"[66]). From such a series of images, one can compute image differences that emphasize those regions of the samples that are rich in a specific compound. As seen in Fig. 7, only $RuO_2 \cdot xH_2O$ displays an absorption peak below 530.5 eV. Thus, the difference in images recorded on the $RuO_2 \cdot xH_2O$ peak at 529.5 eV and below that peak at 527.0 eV identifies those regions of the composite membrane that are

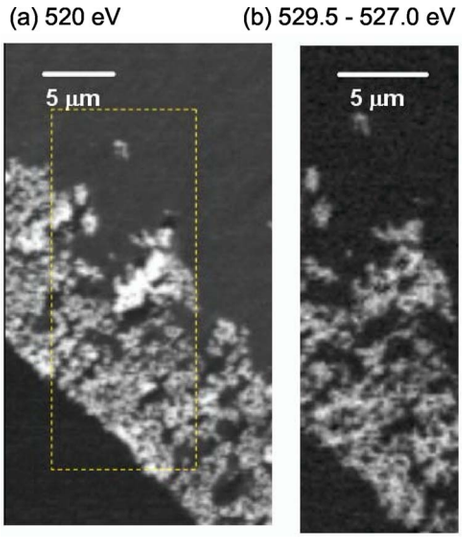

Figure 8. (a) STXM image (o.d.) at 520 eV of a region of a recast Nafion/5% $RuO_2{\cdot}1H_2O$ membrane in the region of the sedimentation layer. (b) Image difference indicating the spatial distribution of the RuO_2.

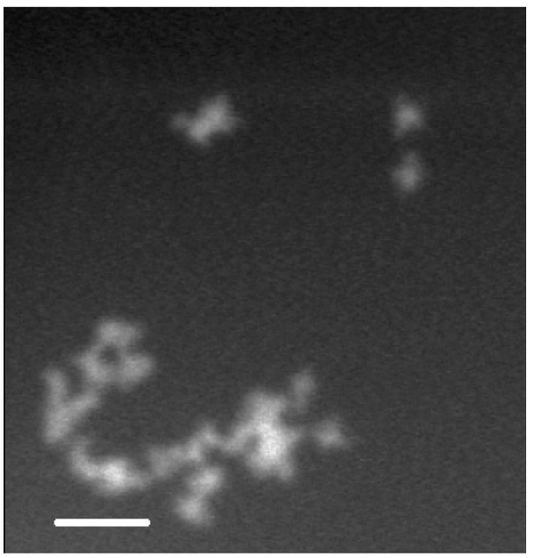

Figure 10. Optical density image at 520 eV of $RuO_2{\cdot}xH_2O$ aggregates in a Nafion/5% $RuO_2{\cdot}xH_2O$ composite membrane measured by STXM far from the sedimentation layer. Scale bar is 1 μm.

$RuO_2{\cdot}xH_2O$-rich. Figure 8b shows this image difference. It shows that $RuO_2{\cdot}xH_2O$ is mainly concentrated at the surface of the membrane. This side of the membrane corresponds to the one that was in contact with the glass slide during the casting procedure. This is consistent with the previous EDX analysis, showing that one side of the composite membrane was enriched with a ruthenium-based compound. The thickness of the $RuO_2{\cdot}xH_2O$ layer at the surface of the membrane is ~7 μm.

Turning now to the bulk of the membrane, we have examined several areas of this sample away from the surface of the membrane in order to look for $RuO_2{\cdot}xH_2O$ outside of the surface layer that is $RuO_2{\cdot}xH_2O$-rich due to sedimentation during the membrane preparation. An image sequence (50 × 150 pixels) from 526 to 560 eV of the whole region displayed in Fig. 8b was recorded. From this data, the O K-edge spectrum of any region can be extracted. Figure 9 presents the O K-edge spectrum of a region far away from the surface of the membrane, along with its spectra decomposition, based on a least-squares fit to the two spectra displayed in Fig. 7. In the O K-edge absorption region, the absorption spectrum of the polymer backbone, which is made of C, F, and S atoms, contributes only to the background signal. As seen from a comparison of the curves, the absorption features of the bulk membrane lying below the absorption threshold cannot be accounted for solely by the signal from the SO_3^- and two ether groups of Nafion. Instead, a small amount of $RuO_2{\cdot}xH_2O$ must be included to reproduce the absorption curve of the bulk membrane. This analysis indicates the bulk of the composite membrane contains up to the equivalent of 0.2 vol % of $RuO_2{\cdot}xH_2O$ (5 nm of an ~ 2500 nm thick membrane).

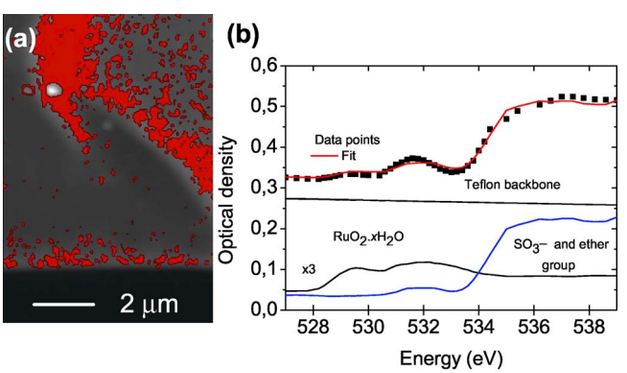

Figure 9. (Color online) (a) Sum of an O K-edge image sequence (520–560 eV) recorded far from the sedimentation layer. The red overlay indicates where the spectrum analyzed in (b) was obtained (it corresponds to pixels with more than 3 nm thickness of RuO_2 but excludes the discrete $RuO_2{\cdot}xH_2O$ particles. (b) Fit to the extracted spectrum. The contribution of the Nafion backbone was estimated from its elemental constituents and tabulated elemental X-ray absorption coefficients. The spectra of $RuO_2{\cdot}xH_2O$ and of SO_3^- and the two ether O of Nafion are those displayed in Fig. 7 but are weighted by the fit coefficients. Note the 3× gain on the $RuO_2{\cdot}xH_2O$ component, which was included for clarity.

We have looked more specifically at the presence of $RuO_2{\cdot}xH_2O$ in the bulk of the membrane, taking full advantage of the spectroscopic and spatial resolution capabilities of STXM. Figure 10 shows an image of several particles of RuO_2 that are located in the bulk of the composite membrane and that are aggregated together. Point spectra taken at that location confirm that these objects are $RuO_2{\cdot}xH_2O$. As seen in Fig. 10, the smallest distinguishable structure has a diameter of about 100–300 nm and several of these small particles are aggregated together to form a larger irregular framework structure with typical dimensions of a few micrometers. As seen in Fig. 10, this aggregate is totally surrounded by Nafion and is isolated from other $RuO_2{\cdot}xH_2O$ particles. The presence of such aggregates of $RuO_2{\cdot}xH_2O$ within the bulk of the membrane confirms that part of the $RuO_2{\cdot}xH_2O$ particles that are mixed with Nafion are indeed trapped in the bulk of the membrane and do not sediment like most of other $RuO_2{\cdot}xH_2O$ particles.

Discussion

Nafion-ruthenium oxide composite membranes have been prepared. Four-probe EIS showed that the in-plane conductivity of the composite Nafion membrane is increased by the addition of $RuO_2{\cdot}xH_2O$. As depicted in Fig. 3, the conductivity of the composite membrane increases as the degree of hydration of $RuO_2{\cdot}xH_2O$, x, decreases. Also, the conductivity of the composite membranes is virtually unchanged as RH is varied. Furthermore, ion-exchange of protons with Na^+ or Ba^{2+} has no effect on the conductivity of Nafion/5% $RuO_2{\cdot}xH_2O$ membranes, as it is observed (and expected)

with a bare Nafion membrane. Both observations raised some concerns regarding the role of electronic conduction in the in-plane conductivity of the composite membrane.

Extensive characterization of the chemical profile composition of the composite membranes has revealed that the fabrication process yields to the sedimentation of $RuO_2{\cdot}xH_2O$ on one side of the membrane. Typically, a layer of about 5–10 μm exists on one side of the membrane, where the concentration of $RuO_2{\cdot}xH_2O$ far exceeds that observed in the bulk. Remembering that $RuO_2{\cdot}xH_2O$ is an electron and a proton conductor, the presence of a sedimentation layer of $RuO_2{\cdot}xH_2O$ on one side of the membrane could be responsible for the occurrence of an electronic conduction path in the composite membrane.

To test this hypothesis, we have estimated the electronic conductivity of the $RuO_2{\cdot}xH_2O$ sedimentation layer, assuming that the experimentally measured resistance value of each Nafion/$RuO_2{\cdot}xH_2O$ membrane was due to the oxide layer and that the thickness of the sedimentation layer was 8 μm. In the case of Nafion/$RuO_2{\cdot}2.12H_2O$, the resistance value at RH = 20% was considered because the conductivity of the bare Nafion is one order of magnitude lower at that RH value (see Fig. 2). The estimated electronic conductivity of the $RuO_2{\cdot}xH_2O$ sedimentation layer would be 3.3, 1.7, and 0.17 S cm^{-1} for x = 0.0, 0.51, and 2.12, respectively.

The observed variation of the electronic conductivity with the hydration level of $RuO_2{\cdot}xH_2O$ is in accordance with literature. For example, Zheng et al.[54] have shown that the resistivity (conductivity) of $RuO_2{\cdot}xH_2O$ decreases (increases) with x. The resistivity of $RuO_2{\cdot}xH_2O$ heated at 300°C (x = 0.11) is 1.36 mΩ cm (corresponding to a conductivity of ~700 S cm^{-1}), while that of as-prepared $RuO_2{\cdot}xH_2O$ (x = 2.00) is more than ten times higher at 21.6 mΩ cm (corresponding to a conductivity of ~50 S cm^{-1}). However, the conductivity values we calculated are lower than that found in Ref. 54. This is not surprising, considering there is a large uncertainty in the determination of the thickness of the sedimentation layer and that our conductivity values were not obtained from measurements on dense pellets, such as in Ref. 54.

Measurements were also performed in bench scale fuel cell test stations, and the performances of composite membranes exceeded that of bare Nafion membrane. This is most particularly evident in the ohmic region, where the membrane's resistance decreases from 0.32 to 0.26 Ω cm^2 as a result of the presence of $RuO_2{\cdot}xH_2O$. This amelioration of the membrane properties is associated with a decrease of the through-plane membrane resistance. As shown by STXM analysis, a non-negligible fraction of $RuO_2{\cdot}xH_2O$ is incorporated in the bulk of the membrane. The precise amount of $RuO_2{\cdot}xH_2O$ incorporated in the membrane bulk is difficult to evaluate from the STXM data, because the complete membrane was not surveyed. However, in the three areas examined, the $RuO_2{\cdot}xH_2O$ amount was equivalent to 4 nm in an ~1000 nm thick membrane, or a 0.4 vol %. This estimation is consistent with the one made from a mass balance calculation, taking into account the thickness of the sedimentation layer and the mass of $RuO_2{\cdot}xH_2O$ used in the membrane preparation. Following that route, we estimated that the actual oxide content in the bulk of the membrane (excluding the sedimentation layer) is less than 1 wt % (or <0.5 vol % based on the densities of the material). Both values are well below the percolation threshold for electronic conduction, and it is not expected that this mechanism is responsible for the decrease of the through-plane resistance of the composite membrane during its operation in real fuel cell test conditions. Consistently, the OCP of fuel cells made with Nafion/$RuO_2{\cdot}xH_2O$ membranes is identical to that observed with pure Nafion membrane, which indicates that short-circuiting between the anode and the cathode is not an issue with these composite membranes. So, we can conclude that through-plane proton conduction in composite Nafion membranes is improved by the presence of $RuO_2{\cdot}xH_2O$ particles in the bulk of the membrane. This would presume that proton conduction in $RuO_2{\cdot}xH_2O$ particles is facilitated compared to bare Nafion.

Extensive research about the close relationships between the structure and the electrochemical properties of $RuO_2{\cdot}xH_2O$ has established that this compound is a mixed protonic/electronic conductor, whose high pseudocapacitance can actually be ascribed to reversible redox processes with simultaneous exchange of protons and electrons.[41] As shown by Sugimoto et al.,[67] electronic conduction in $RuO_2{\cdot}xH_2O$ is not a limiting factor. The proton transport properties of $RuO_2{\cdot}xH_2O$ have been studied by solid-state ^1H nuclear magnetic resonance (NMR).[42] It was shown that the activation energy for proton transport, E_a, in $RuO_2{\cdot}xH_2O$ annealed at 150°C is minimal and that it increases for $RuO_2{\cdot}xH_2O$ annealed at lower or higher temperature. The lowest E_a value reported for $RuO_2{\cdot}xH_2O$ heated at 150°C is ~2.4 kJ/mol. For comparison, Ye et al.[68] measured the activation energy for proton transport in Nafion and Nafion composites (SiO_2-Nafion and ZrP-Nafion), using the same solid-state ^1H NMR technique. The E_a value of dried Nafion is 16.4 kJ/mol, while that of hydrated Nafion is 11.0 kJ/mol. In the case of Nafion composites, the E_a value is 12.2 and 10.3 kJ/mol for SiO_2-Nafion and ZrP-Nafion, respectively. The activation energy for proton transport in Nafion and Nafion composites is at least four times higher than the minimal E_a value of $RuO_2{\cdot}xH_2O$ heated at 150°C. Even in the case of $RuO_2{\cdot}xH_2O$ heated at 300°C (dehydrated RuO_2, E_a = 4.9 kJ/mol), the E_a values of Nafion and Nafion composites are a factor of two higher. All these values are consistent with the fact that the introduction of $RuO_2{\cdot}xH_2O$ particles in the bulk of the Nafion membrane should yield to a decrease of the through-plane membrane resistance.

As pointed out by Ye et al.,[68] the activation energy arising from NMR measurements of proton dynamics are extremely local, molecular probes of proton mobility. One can hardly estimate the through-plane resistance of a Nafion/$RuO_2{\cdot}xH_2O$ composite membrane from such values. This is especially so in our case, where the particle size distribution and the spatial arrangement of the $RuO_2{\cdot}xH_2O$ particles in the bulk of the membrane is not known.

Conclusion

The previous measurements hold the promise that the mixing of Nafion with $RuO_2{\cdot}xH_2O$ particles could effectively yield to the preparation of composite membrane with improved properties compared to bare Nafion. Also, proton conduction in $RuO_2{\cdot}xH_2O$ does not depend on external humidification and much could be gained by developing Nafion/$RuO_2{\cdot}xH_2O$ composite membranes that are less dependent on external humidification that the actual bare Nafion membrane. As discussed previously, the activation energy for proton transport in $RuO_2{\cdot}xH_2O$ is minimal at the targeted operating temperature (120–130°C) of PEMFCs. Such improved membranes could also be of great benefit. However, as demonstrated previously, much needs to be done to improve and optimize the preparation procedure, and new ways of mixing and preparing the composite membrane need to be devised to circumvent the sedimentation of the $RuO_2{\cdot}xH_2O$ particles during the casting procedure.

Acknowledgments

This work was financially supported by the National Sciences and Engineering Research Council (NSERC) of Canada, the "Fonds Québécois de la Recherche sur la Nature et les Technologies" (FQRNT).

Institut National de la Recherche Scientifique–Énergie, Matériaux et Télécommunications assisted in meeting the publication costs of this article.

References

1. W. H. J. Hogarth, J. C. Diniz da Costa, and G. Q. Lu, *J. Power Sources*, **142**, 223 (2005).
2. Q. Li, R. He, J. O. Jensen, and N. J. Bjerrum, *Chem. Mater.*, **15**, 4896 (2003).
3. B. Smitha, S. Sridhar, and A. A. Khan, *J. Membr. Sci.*, **259**, 10 (2005).
4. O. Savadogo, *J. Power Sources*, **127**, 135 (2004).
5. S. Wasmus, A. Valeriu, G. D. Mateescu, D. A. Tryk, and R. F. Savinell, *J. Membr. Sci.*, **185**, 105 (2001).
6. S. Malhotra and R. Datta, *J. Electrochem. Soc.*, **144**, L23 (1997).
7. B. Bahar, A. R. Hobson, J. A. Kolde, and D. Zuckerbrod, U.S. Pat. 5,547,551

(1996).
8. V. Ramani, H. R. Kunz, and J. M. Fenton, *J. Membr. Sci.*, **232**, 31 (2004).
9. V. Ramani, H. R. Kunz, and J. M. Fenton, *J. Membr. Sci.*, **266**, 110 (2005).
10. V. Ramani, H. R. Kunz, and J. M. Fenton, *J. Membr. Sci.*, **279**, 506 (2005).
11. V. Ramani, H. R. Kunz, and J. M. Fenton, *Electrochim. Acta*, **50**, 1181 (2005).
12. V. Ramani, H. R. Kunz, and J. M. Fenton, *J. Power Sources*, **152**, 182 (2005).
13. P. Staiti, A. S. Aricó, V. Baglio, F. Lufrano, E. Passalacqua, and V. Antonucci, *Solid State Ionics*, **145**, 101 (2001).
14. M. Doyle, S. K. Choi, and G. Proulx, *J. Electrochem. Soc.*, **147**, 34 (2000).
15. W. Liu, K. Ruth, and G. Rush, *J. New Mater. Electrochem. Syst.*, **4**, 227 (2001).
16. Y. Si, H. R. Kunz, and J. M. Fenton, *J. Electrochem. Soc.*, **151**, A623 (2004).
17. R. Jiang, H. R. Kunz, and J. M. Fenton, *Electrochim. Acta*, **51**, 5596 (2006).
18. X.-B. Zhu, H.-M. Zhang, Y.-M. Liang, Y. Zhang, and B.-L. Yi, *Electrochem. Solid-State Lett.*, **9**, A49 (2006).
19. L. Wang, D. M. Xing, Y. H. Liu, Y. H. Cai, Z.-G. Shao, Y. F. Zhai, H. X. Zhong, B. L. Yi, and H. M. Zhang, *J. Power Sources*, **161**, 61 (2006).
20. M. Li, Z.-G. Shao, H. Zhang, Y. Zhang, X. Zhu, and B. Yi, *Electrochem. Solid-State Lett.*, **9**, A92 (2006).
21. B. Baradie, J. P. Dodelet, and D. Guay, *J. Electroanal. Chem.*, **489**, 101 (2000).
22. K. A. Mauritz, *Mater. Sci. Eng., C*, **6**, 121 (1998).
23. R. A. Zoppi and S. P. Nunes, *J. Electroanal. Chem.*, **445**, 39 (1998).
24. K. T. Adjemian, S. J. Lee, S. Srinivasan, J. Benziger, and A. B. Bocarsly, *J. Electrochem. Soc.*, **149**, A256 (2002).
25. N. Miyake, J. S. Wainright, and R. F. Savinell, *J. Electrochem. Soc.*, **148**, A898 (2001).
26. F. Damay and L. C. Klein, *Solid State Ionics*, **162–163**, 261 (2003).
27. Z.-G. Shao, P. Joghee, and I.-M. Hsing, *J. Membr. Sci.*, **229**, 43 (2004).
28. Z.-G. Shao, H. Xu, M. Li, and I.-M. Hsing, *Solid State Ionics*, **177**, 779 (2006).
29. T. M. Thampan, N. H. Jalani, P. Choi, and R. Datta, *J. Electrochem. Soc.*, **152**, A316 (2005).
30. A. S. Aricó, V. Baglio, A. Di Blasi, P. Creti, P. L. Antonucci, and V. Antonucci, *Solid State Ionics*, **161**, 251 (2003).
31. A. Saccà, A. Carbone, E. Passalacqua, A. D'Epifanio, S. Licoccia, E. Traversa, E. Sala, F. Traini, and R. Ornelas, *J. Power Sources*, **152**, 16 (2005).
32. P. Liu, J. Bandara, Y. Lin, D. Elgin, L. F. Allard, and Y.-P. Sun, *Langmuir*, **18**, 10398 (2002).
33. H. Uchida, Y. Ueno, H. Hagihara, and M. Watanabe, *J. Electrochem. Soc.*, **150**, A57 (2003).
34. W. G. Grot and G. Rajendra, U.S. Pat. 5,919,583 (1998).
35. P. Costamagna, C. Yang, A. B. Bocarsly, and S. Srinivasan, *Electrochim. Acta*, **47**, 1023 (2002).
36. C. Yang, S. Srinivasan, A. B. Bocarsly, S. Tulyani, and J. B. Benziger, *J. Membr. Sci.*, **237**, 145 (2004).
37. H.-C. Kuan, C.-S. Wu, C.-Y. Chen, Z.-Z. Yu, A. Dasari, and Y.-W. Mai, *Electrochem. Solid-State Lett.*, **9**, A76 (2006).
38. M. Watanabe, H. Uchida, Y. Seki, M. Emori, and P. Stonehart, *J. Electrochem. Soc.*, **143**, 3847 (1996).
39. M. Watanabe, H. Uchida, and M. Emori, *J. Electrochem. Soc.*, **145**, 1137 (1998).
40. H. Hagihara, H. Uchida, and M. Watanabe, *Electrochim. Acta*, **51**, 3979 (2006).
41. *Proton Conductors: Solids, Membranes and Gels—Materials and Devices*, P. Colomban, Editor, Cambridge University Press, Cambridge, MA (1992).
42. R. Fu, Z. Ma, and J. P. Zheng, *J. Phys. Chem. B*, **106**, 3592 (2002).
43. W. Dmowski, T. Egami, K. E. Swider-Lyons, C. T. Love, and D. R. Rolison, *J. Phys. Chem. B*, **106**, 12677 (2002).
44. C.-C. Hu, W.-C. Chen, and K.-H. Chang, *J. Electrochem. Soc.*, **151**, A281 (2004).
45. W. Sugimoto, H. Iwata, K. Yokoshima, Y. Murakami, and Y. Takasu, *J. Phys. Chem. B*, **109**, 7330 (2005).
46. I.-H. Kim and K.-B. Kim, *J. Electrochem. Soc.*, **153**, A383 (2006).
47. R. B. Moore III and C. R. Martin, *Anal. Chem.*, **58**, 2569 (1986).
48. R. B. Moore III and C. R. Martin, *Macromolecules*, **21**, 1334 (1988).
49. P. Dimitrova, K. A. Friedrich, B. Vogt, and U. Stimming, *J. Electroanal. Chem.*, **532**, 75 (2002).
50. V. Baglio, A. S. Arico, A. DiBlasi, V. Antonucci, P. L. Antonucci, S. Licoccia, E. Traversa, and F. Serraino Fiory, *Electrochim. Acta*, **50**, 1241 (2005).
51. P. C. Rieke and N. E. Vanderborgh, *J. Membr. Sci.*, **32**, 313 (1987).
52. S. Gottesfeld and T. A. Zawodzinski, in *Advances in Electrochemical Science and Engineering*, Vol. 5, R. C. Alkire, H. Gerischer, D. M. Kolb, and C. W. Tobias, Editors, p. 220, Viley-VCH, Weinheim (1997).
53. K.-H. Chang and C.-C. Hu, *J. Electrochem. Soc.*, **151**, A958 (2004).
54. J. P. Zheng, P. J. Cygan, and T. R. Jow, *J. Electrochem. Soc.*, **142**, 2699 (1995).
55. O. Barbieri, M. Hahn, A. Foelske, and R. Kötz, *J. Electrochem. Soc.*, **153**, A2049 (2006).
56. D. A. McKeown, P. L. Hagans, L. P. L. Carette, A. E. Russell, K. E. Swider, and D. R. Rolison, *J. Phys. Chem. B*, **103**, 4825 (1999).
57. Q. L. Fang, D. A. Evans, S. L. Robertson, and J. P. Zheng, *J. Electrochem. Soc.*, **148**, A833 (2001).
58. L. A. Zook and J. Leddy, *Anal. Chem.*, **68**, 3793 (1996).
59. Y. Sone, P. Ekdunge, and D. Simonsson, *J. Electrochem. Soc.*, **143**, 1254 (1996).
60. A. L. D. Kilcoyne, T. Tylisczak, W. F. Steele, S. Fakra, P. Hitchcock, K. Franck, E. Anderson, B. Harteneck, E. G. Rightor, G. E. Mitchell et al., *J. Synchrotron Radiat.*, **10**, 125 (2003).
61. T. Warwick, H. Ade, A. L. D. Kilcoyne, M. Kritscher, T. Tylisczcak, S. Fakra, A. P. Hitchcock, P. Hitchcock, and H. A. Padmore, *J. Synchrotron Radiat.*, **9**, 254 (2002).
62. H. Ade, in *Experimental Methods in the Physical Sciences*, Vol. 32, J. A. R. Samson and D. L. Ederer, Editors, p. 225, Academic Press, New York (1998).
63. H. Ade and S. G. Urquhart, in *Chemical Applications of Synchrotron Radiation* T. K. Sham, Editor, World Scientific Publishing, Singapore (2002).
64. aXis2000, written in Interactive Data Language, is freeware available for noncommercial use at http://unicorn.mcmaster.ca/aXis2000.html
65. K. R. Wilson, M. Cavalleri, B. S. Rude, R. D. Schaller, A. Nilsson, L. G. M. Pettersson, N. Goldman, T. Catalano, J. D. Bozek, and R. J. J. Saykally, *J. Phys.: Condens. Matter*, **14**, L221 (2002).
66. C. Jacobsen, S. Wirick, G. Flynn, and C. Zimba, *J. Microsc.*, **197**, 173 (2000).
67. W. Sugimoto, H. Iwata, K. Yokoshima, Y. Murakawi, and Y. Takasu, *J. Phys. Chem.*, **109**, 7330 (2005).
68. G. Ye, N. Janzen, and G. R. Goward, *Macromolecules*, **39**, 3283 (2006).